JOURNAL OF SOLID STATE CHEMISTRY 77, 33–39 (1988)

Experimental Evidence of the Ramsdellite–Rutile Intergrowth Model in Electrolytic γ-MnO_2

JEAN CLAUDE CHARENTON AND PIERRE STROBEL

Laboratoire de Cristallographie CNRS, associé à l'USTMG, 166X-38042 Grenoble, France

Received January 18, 1988; in revised form May 5, 1988

Electrolytical synthesis allowed the synthesis of γ-MnO_2 samples with grain size suitable for single-crystal electron diffraction for the first time. The diffraction patterns consist of sets of strong, sharp reflections and additional weak, broad reflections. While the former are compatible with both the γ-MnO_2 (orthorhombic cell) and ε-MnO_2 (hexagonal cell) structures, the observed extinctions and the weak spot patterns are totally consistent with a structural model proposed by P. M. De Wolff [*Acta Crystallogr.* **12,** 341 (1959)] and consisting of an intergrowth of pyrolusite (rutile-type) and ramsdellite domains. The position of reflections with k odd allows an estimate of the fraction of pyrolusite blocks, which can vary within a given sample.

Introduction

The structure of γ-MnO_2, the nonstoichiometric form of manganese dioxide widely used in the battery industry, has long been a debated topic (*1, 2*). Battery-active γ-MnO_2 is prepared either by electrolysis or by aqueous redox chemistry (giving the so-called "electrolytical" or "chemical" manganese dioxide (EMD or CMD), respectively). It is usually identified by a powder X-ray diffraction pattern containing only four typical (and rather broad) lines at $d \approx 400$, 241, 213, and 163 pm. Structural studies have been hindered by the variable composition and probable disorder, and the poor thermal stability of this compound, which has so far prevented crystal growth and in some cases led to decomposition in electron microscope environments (*3*).

The most convincing X-ray work to date is that of De Wolff (*4*). From the study of earlier line-rich powder diagrams, this author proposed a structural model based on intergrowth of two known forms of manganese dioxide, ramsdellite (orthorhombic) and pyrolusite (rutile-type) (for a review of these structures, see, for example, Ref. (*1*)). However, experimental evidence confirming his model has been scarce. For the natural mineral *nsutite,* which is believed to be structurally related to γ-MnO2 (*1*), careful IR studies supported De Wolff's model (*5*), while high-resolution transmission electron microscopy revealed a mixture of more complex intergrowth patterns, together with noncoherent defects (*6*). Very recently, grains of γ-MnO2 with De Wolff's structure were identified as a minor phase in natural crystals of pyrolusite (*7*).

A quite different structure has been put

0022-4596/88 $3.00

forward for lamellar or fibrous synthetic material obtained by electrolysis under specific conditions. From X-ray diffraction on oriented grains, De Wolff *et al.* (*8*) concluded in favor of a small hexagonal cell, based on a compact packing of oxide anions, with random occupation of half the octahedral sites by manganese atoms. In view of this rather different arrangement, a new name (ε-MnO_2) was proposed for this compound (*8*). Its cell is compatible with three of the four typical X-ray lines of γ-MnO_2.

In a previous paper, Strobel *et al.* (*9*) presented electron diffraction evidence of at least three distinct structures in various industrial samples of γ-MnO_2 and homemade CMDs. The purpose of the present paper is to provide further experimental diffraction data on several γ-MnO_2 samples prepared electrolytically (EMD), and to show that diffraction patterns previously reported as hexagonal fit De Wolff's intergrowth model better. The superstructure reflections allow us to estimate the fractions of pyrolusite and ramsdellite domains. This is the first experimental observation of De Wolff's intergrowth structure in synthetic γ-MnO_2.

Experimental

γ-MnO_2 samples of various origins (*9*, *10*) were studied. Those suitable for electron diffraction belong to three groups:

(i) a CMD obtained by calcination of freshly precipitated manganese carbonate at 400°C in air followed by leaching for 2 hr in 3 *M* nitric acid at 90°C (sample 9 in Ref. (*9*), hereafter named CMD9);

(ii) an international manganese dioxide standard "ICS 2" (Japanese EMDs), supplied by the International Battery Association (*10*);

(iii) EMDs prepared by us by electrolysis (*9*).

The experimental conditions were the following: manganese chloride solutions (100 g/liter) in hydrochloric medium at pH $\approx$ 1, temperature 90–100°C, current densities equal to 1.0 (sample EMD1) or 0.023 A/dm^2 (sample EMD2). The preparation conditions for the latter correspond to those reported for the deposition of "ε-MnO_2" (*11*).

Chemical compositions were deduced from two analytical determinations: (i) total manganese content, by atomic absorption after dissolution in hot hydrochloric acid, and (ii) manganese average oxidation state, by oxalate redox titration in sulfuric medium (*11*). Water contents were then obtained by difference. Thermogravimetry has also been carried out (*9*); it is unreliable for determining water contents, because no plateau is observed before the beginning of oxygen loss. Powder X-ray patterns were recorded on a Philips diffractometer with Cu $K\alpha$ radiation at 0.25°/min scan speed with internal silicon standards. Specimens for electron microscopy were ground under acetone and deposited on a copper grid covered with a thin holey carbon film. They were studied using a Philips 400T electron microscope fitted with a double-tilt goniometer and operated at 120 kV.

Results

1. Chemical and X-Ray Characterization

Chemical compositions and characteristics of the powder X-ray diagrams are given in Table I. Composition variations between the three kinds of samples are rather small. X-ray powder patterns are consistent with the usual γ-MnO_2 line quartet. EMD1, however, does not exhibit the 400-pm line, but instead a wide bump around 420 pm. The half-peak widths of diffraction lines increase in the order EMD2 < EMD1 $\ll$ CMD9. The powder diagrams of EMD1 and EMD2 (*13*) exhibit more than 12 diffraction lines, in contrast with CMDs and industrial

TABLE I

CHEMICAL AND STRUCTURAL CHARACTERIZATION OF SAMPLES

Sample	Origin	Composition	X-ray pattern n^a	ΔW^b (pm) 400	241	212	163	Grain size (μm)
CMD9	Sample 9 in Ref. (*9*)	$MnO_{1.93(4)}H_2O_{0.26(6)}$	4	4.5	0.8	1.5	2.2	0.1 × 0.4
ICS2	EMD standard	$MnO_{1.98}H_2O_{\approx 0.28}$ (*10*)	4	2.4	0.7	0.8	1.0	Mostly <0.05 + 0.03 × 0.15
EMD1	Electrolysis, high J^c	$MnO_{1.94(4)}H_2O_{0.25(6)}$	11	3.0 (423 pm)	0.4	0.6	0.9	0.4–0.6
EMD2	Electrolysis, low J	$MnO_{1.98(4)}H_2O_{0.31(6)}$	18	1.0	0.3		0.3	0.6, 1.0 × 0.3

[a] Number of lines observed.
[b] Half-peak width in degrees.
[c] J = current density.

EMDs studied previously (*9*). These features indicate that EMD1 and EMD2 have larger crystal sizes or a higher crystallinity (or both) than usual synthetic γ-MnO_2 samples; this trend is favored by low current densities. The morphological observation in electron microscopy confirms this (see grain sizes in Table I).

The powder diagrams of EMD1 and EMD2 are compatible with De Wolff's orthorhombic intergrowth model (*4*), neglecting the bump near 420 pm in EMD1. In the absence of the 400-pm line, the latter can also be indexed in the hexagonal ε-MnO_2 cell. Least-squares refined cell parameters are compared to those of De Wolff in Table II. These samples look fibrous, as previously reported for ε-MnO_2 (*11*); the fiber direction is perpendicular to the electrode surface.

2. *Electron Diffraction*

Samples EMD1, EMD2, and CMD all contain columnar or bean-shaped crystals larger than ≈0.3 μm, giving single-crystal electron diffraction patterns. EMD1 grains gave the hexagonal diagram (Fig. 1a) already observed in CMD9 (*9*), corresponding either to the zone axis $[100]_h$ or $[100]_o$ (where the subscripts h and o refer to De Wolff's hexagonal (ε-MnO_2) and orthorhombic (γ-MnO_2) models, respectively). Figure 1b, obtained by tilting the sample around b_o, shows intense reflections as well as diffuse spots at one-third of the reciprocal distance d^* between the intense spots along the rotation axis.

For EMD2, the diffraction plane shown in Fig. 2a is not indexable in the hexagonal cell, because of the weak reflections indicated by arrows. Rotation around b_o yields diffraction patterns containing intense reflections with $(l_o + k_o/2)$ even (Fig. 2b), while reflections corresponding to k_o odd are weaker and more diffuse. The recipro-

TABLE II

STRUCTURAL DATA ON CRYSTALLIZED EMDS

Sample	X-ray cell parameters (pm) a	b	c	Odd k reflections shift (see text)	p^a
D in Ref. (*4*)	445	930	285	0.14*b*	0.25
E in Ref. (*4*)				0.05*b*	0.12
EMD2	440	939	283	0.04*b*	0.10
				0.09*b*	0.18
EMD1	443	938	283		0.5
or hexagonal	280		443		
ε-MnO_2(8)	280		445 (Hexagonal)		

[a] Fraction of pyrolusite blocks.

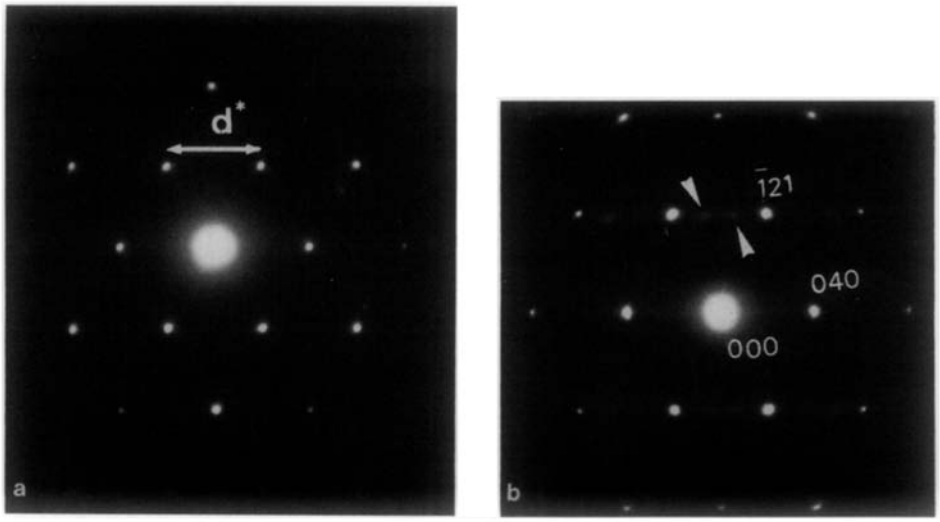

FIG. 1. Electron diffraction patterns of EMD 1: zone axis [100] (a), [101] (b).

cal distance between "(010)" and the central spot seems to vary from grain to grain and can be estimated to lie between 0.04 and 0.09b (see Figs. 2b and 2c).

The CMD9 sample gave diffractions patterns very similar to those of EMD2 (*9*). The international standard ICS2 had much smaller grain size, yielding mostly ring (polycrystal) diffraction diagrams with $d \approx 245$ and 163 pm. Single-crystal diffraction could be observed on some grains of ICS 2 (elongated grains $\approx 0.03 \times 0.15$ μm) and corresponded to the orthorhombic cell (*10*).

Discussion

1. De Wolff's Intergrowth Model

In the X-ray powder diagram of line-rich γ-MnO_2s, indexing in an orthorhombic cell close to that of ramsdellite gives sharp reflections obeying the condition $(l_o + k_o/2)$ even, while the k odd lines are broad. These findings are the basis of De Wolff's structural model, using a ramsdellite–pyrolusite intergrowth (*4*). Both structures are shown in Fig. 3. Rutile contains tunnels of square section ("1 × 1" tunnels) along c, edged by chains of corner-sharing MnO_6 octahedra. Ramsdellite contains double chains along c, leading to tunnels of rectangular section ("1 × 2" tunnels). (The size of these tunnels makes possible the occupation of tunnels sites by other cations or water molecules, as in γ-MnO_2.) The stacking of octahedra differs along b only, so that pyrolusite and ramsdellite blocks can be connected via ac planes (Fig. 4). In De Wolff's model, if ramsdellite double chains are defined by an (a,b,c) unit cell, the addition of one layer of single (pyrolusite) chains defines a second unit cell (a,b',c) with $b' = \frac{3}{4}b + c/2$. Note that this model is valid only for isolated layers of pyrolusite (pyrolusite fraction $p < \frac{1}{2}$).

The Ramsdellite and combined cells are shown in the reciprocal plane b^*c^* in Fig. 5 (*4*). Their Miller indices are related by $h' = h$, $k' = \frac{3}{4}k + \frac{1}{2}l$, $l' = l$. Introducing a different b' translation in the ramsdellite cell results in a shift of the intense and sharp (hkl) diffraction spots toward the closest $(h'k'l')$ spots, with a simultaneous broadening of the spots along k. The shift and broadening increase with increasing concentration of pyrolusite blocks p.

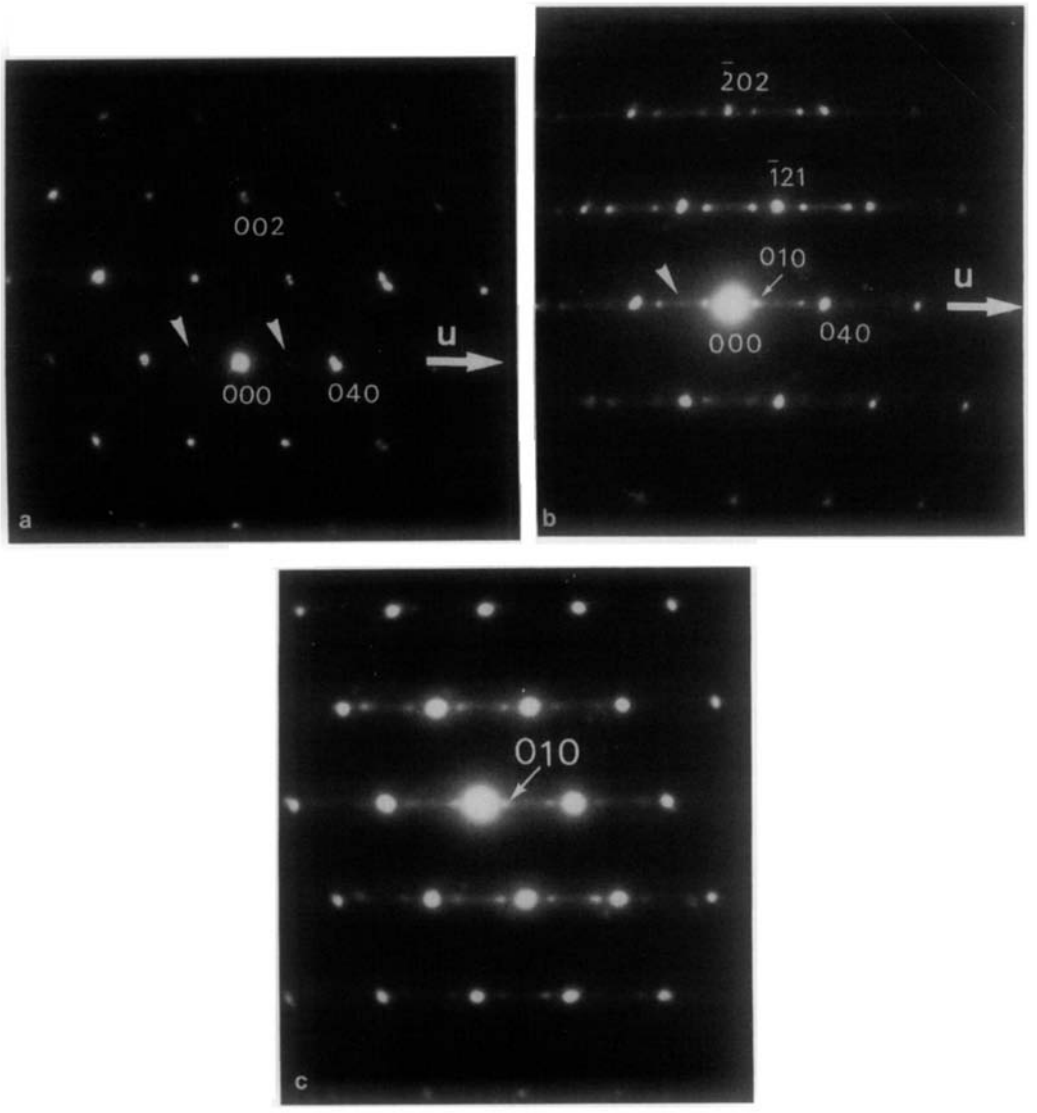

FIG. 2. Electron diffraction patterns of EMD 2: zone axis [100] (a); [101] (b); same as (b), from a different grain (c).

Within this model, the $(l + k/2)$ even reflections are never shifted or broadened. $(l + k/2)$ odd reflections, located between two $(h'k'l')$ spots, are not shifted, but are broadened and disappear with increasing p. Finally, all reflections with k odd have a neighboring reflection at $\frac{1}{3}b^*$ along b^*, which are shifted as shown by the arrows in Fig. 5.

2. Comparison with Experimental Data

The electron diffraction diagrams obtained for sample EMD1 are fully compatible with this model. In the [100] plane (Fig. 1a), the condition $(l + k/2)$ even is observed. Figure 1b corresponds to the [101] zone, with again the $(l + k/2)$ odd reflections absent. Diffuse spots are indexable

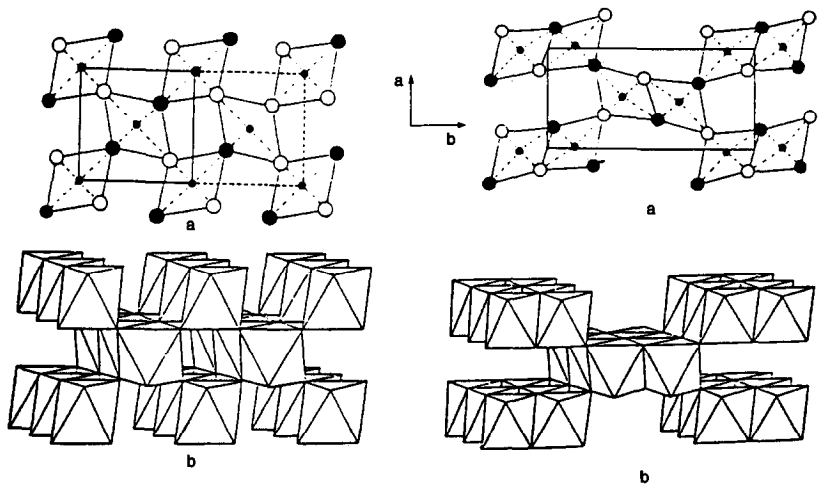

FIG. 3. Structures of pyrolusite/rutile (left) and ramsdellite (right) [from Ref. (*1*)]. (a) *ab*-plane projection (large circles, O; small circles, Mn). (b) Perspective view showing the single and double chains along *c*.

with k odd and are shifted by $b^*/3$, corresponding to the limiting case of the model with $p = \frac{1}{2}$ (equal fractions of ramsdellite and pyrolusite blocks).

For the EMD2 sample, $(l + k/2)$ odd spots are weak and diffuse in both the [100] and [101] diagrams (Fig. 2). The k odd reflections are absent in the [100] plane, and shifted in the direction corresponding to the model in the [101] plane (Fig. 2b). The shift

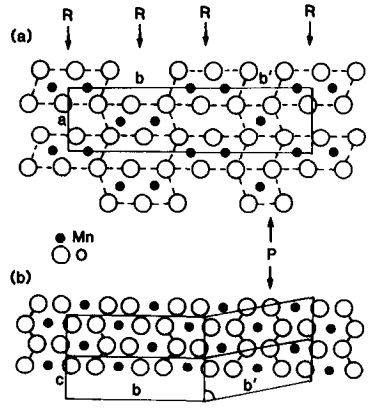

FIG. 4. Intergrowth of ramsdellite (R) and pyrolusite (P) blocks. Projections along *c* (top) and along *a* (bottom) [from Ref. (*4*)].

is variable among different grains (from $0.4b^*$ to $0.09b^*$). In De Wolff's model, these values can be related to the pyrolusite content (*4*) by

$$(1 - 2p) \sin 2\pi r - 2p \cos 3\pi r/2 = 0.$$

Experimental values of p are given in Table II, showing that p can vary in a given sample.

Finally, it should be noted that diagrams such as those in Figs. 1a and 2a are metrically hexagonal, with "a_h" = 285 pm, in good agreement with the possible hexagonal cell deduced from the powder X-ray diagram of EMD1 (Table II). Very similar electron diffraction diagrams were obtained on the CMD9 sample, where the weak spots were not always resolved and appeared as streaks along b^* (*9*). These features had been tentatively assigned to partial ordering in the hexagonal ε-MnO_2 structure, which contains a disordered distribution of manganese atoms (*8*). But the hexagonal cell cannot account for the diffuse spots in [101] planes. Moreover, *all* features corresponding to the model reciprocal space diagram (Fig. 5) are found ex-

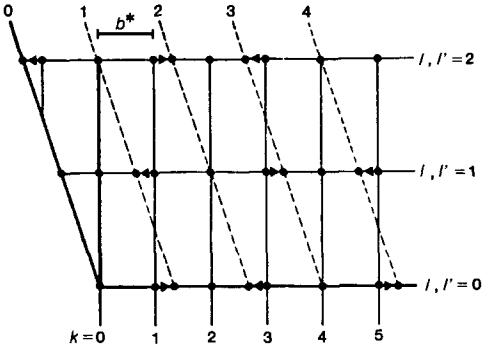

FIG. 5. Schematic drawing of h = constant section of the reciprocal lattice corresponding to De Wolff's model [from Ref. (*4*)]. Full line, ramsdellite pattern; dotted line, pyrolusite pattern.

perimentally. It can be concluded that the synthetic EMDs prepared in this study fully correspond to De Wolff's intergrowth model. Note that these compounds include EMD2, which has been synthesized in conditions previously reported to stabilize the ε-MnO_2 structure. As shown by the CMD9 case, small variations in ordering of manganese cations can result in ambiguous indexation in the latter structure.

Acknowledgments

The authors thank F. De Bergevin, J. L. Hodeau, and D. Tranqui for helpful discussions and M. Perroux for his assistance in electron microscopy.

References

1. R. G. BURNS AND V. B. M. BURNS, "MnO_2 Symposia Proceedings" (A. Kozawa, Ed.), Vol. 1, p. 306, Electrochem. Soc., Cleveland, (1975), and Vol. 2, p. 97 (1980).
2. R. GIOVANOLI, "MnO_2 Symposium Proceedings" (A. Kozawa, Ed.), Vol. 2, p. 113, Electrochem. Soc., Cleveland (1980); *Prog. Batteries Sol. Cells* **2,** 116 (1980).
3. R. GIOVANOLI, R. MAURER, AND W. FEITKNECHT, *Helv. Chem. Acta* **50,** 1072 (1967).
4. P. M. DE WOLFF, *Acta Crystallogr.* **12,** 341(1959).
5. R. M. POTTER AND G. R. ROSSMAN, *Amer. Miner.* **64,** 1199 (1979).
6. S. TURNER AND P. R. BUSECK, *Nature (London)* **304,** 143 (1983).
7. N. YAMADA AND M. OHMASA, International Congress of Crystallography, Perth, Paper C-311 (1987).
8. P. M. DE WOLFF, J. W. VISSER, R. GIOVANOLI, AND R. BRÜTSCH, *Chimia* **32,** 257 (1978).
9. P. STROBEL, J. C. JOUBERT, AND M. J. RODRIGUEZ, *J. Mater. Sci.* **21,** 583 (1986).
10. A. KOZAWA, "3rd MnO_2 Symposium Proceedings," I.B.A. Press, Cleveland, OH (1985).
11. E. PREISLER, *J. Appl. Electrochem.* **6,** 301 (1976).
12. D. A. PANTONY AND A. SIDDIQI, *Talanta* **9,** 811 (1962).
13. J. C. CHARENTON, Thèse, Université Scientifique et Médicale de Grenoble (1987).